

Supplementary Information for

Chemical Characterization of Nanoparticles and Volatiles Present in Mainstream Hookah Smoke

**Véronique Perraud,^{1*} Michael J. Lawler,¹ Kurtis T. Malecha,¹ Rebecca M. Johnson,² David
A. Herman,² Norbert Straimer,³ Michael T. Kleinman,² Sergey A. Nizkorodov¹ and James
N. Smith¹**

¹Department of Chemistry, University of California, Irvine, CA 92697

²School of Medicine, University of California, Irvine, CA 92697

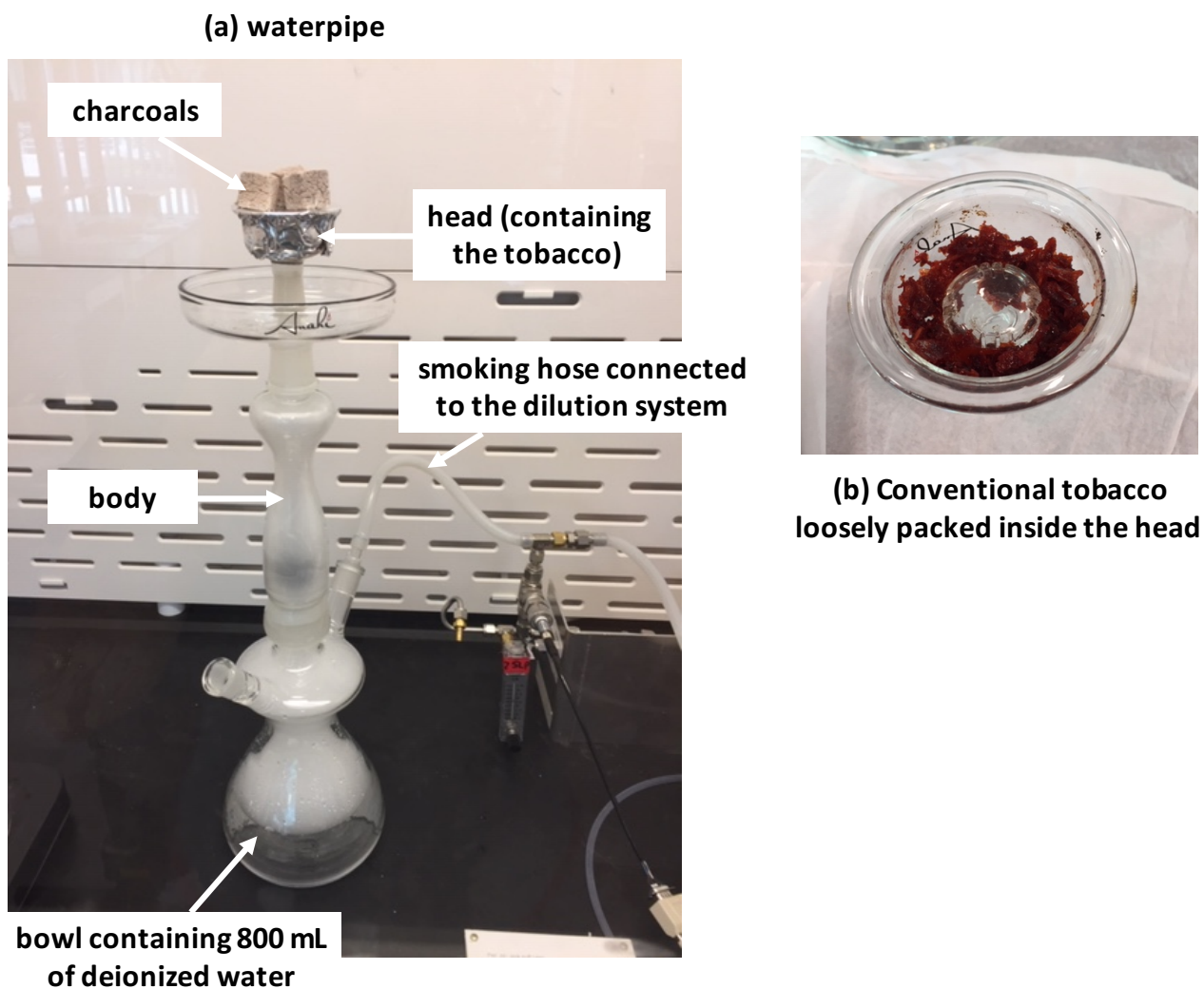
³Department of Epidemiology, University of California, Irvine, California, USA

1. Waterpipe Smoking Protocol

All smoking sessions were performed using the same waterpipe (Anahi Smoke, model

“Fantasy”) described in Figure S1:

Figure S1. (a) Glass waterpipe used in this study. (b) Close-up of the conventional tobacco preparation loosely packed inside the head of the waterpipe.



Prior to an experiment, the glass waterpipe was entirely cleaned using deionized water followed by isopropyl alcohol and kept overnight in an oven maintained at $\sim 100^{\circ}\text{C}$ to evaporate the residual solvents. The preparation of the tobacco mixture was adapted from Shihadeh et al.

(2012) and Shihadeh et al. (2014), where 10 g of tobacco mixture, which were stored in the dark at $\sim 4^{\circ}\text{C}$ until its use, were weighed and left on the bench at room temperature overnight for conditioning. At the beginning of each experiment, 800 mL of deionized water was added to the waterpipe reservoir and the downstem was placed 39 mm under the water surface. Then, the 10 g of prepared tobacco were packed loosely inside the waterpipe head and wrapped with perforated aluminum foil. Three cubes of charcoal were heated on a hot plate for about 10 min, insuring that all the faces of the cube were incandescent. The cubes were then placed on the foil surface atop the tobacco for 5 min prior to the first puff. Three charcoal cubes were necessary to uniformly heat the tobacco. A smoking pump, operating at a total flow rate of $\sim 10\text{ L min}^{-1}$, was connected to a solenoid air control valve (Ingersoll Rand, model P251SS-012-D) that was timed by a control board (Teague Enterprises, model TE-2) and was used to provide a 4 s puff at a frequency of 2 min^{-1} . An additional flow of $\sim 3\text{ L min}^{-1}$ (sum of all the analytical instrument flow rates), yielding a total puff flow rate of $\sim 13\text{ L min}^{-1}$, was drawn into a dilution system as described below. All smoking sessions were executed for 30 min. At the end of the experiment, the remaining tobacco was weighed to estimate the loss of tobacco product for one session.

2. Fast Flow Dilution System

(a) Description. The fast flow dilution system (Figure 1) begins with a two-valve delivery system that selects between sampling $\sim 3\text{ L min}^{-1}$ of the total puff flow, which corresponds to the sum of the inlet flows to all instruments, or the same flow rate of purified air (FTIR purge air generator, Parker Balston model 75-62). This assured that a continuous flow of sample air was

provided to the instruments at all time regardless of whether or not a puff was being made. The use of both valves was simply to increase the air throughput through the system. The valves were synchronized to the puffs using a timing signal provided by the control board. Exiting the two-valve delivery system, the sample was then diluted by a custom two-stage fast flow dilution stainless steel tube (Blair et al. 2015). The puff was diluted first by addition of a dry purified air flow of $\sim 16 \text{ L min}^{-1}$ using a mass flow controller (Sierra Instruments, model SmartTrak 50). A fraction of the diluted flow ($\sim 3 \text{ L min}^{-1}$) was transferred to a second dilution stage through an orifice, where it was diluted by addition of another $\sim 15 \text{ L min}^{-1}$ of dry purified air. Again, only a fraction of that flow ($\sim 3 \text{ L min}^{-1}$) was drawn into a stainless steel mixing chamber, to which sampling tubes for the individual instruments were attached. Each dilution branch was equipped with a critical orifice (O'Keefe Controls Co., Type K2) and HEPA filter (Pall Corp., model 12144) followed by vacuum pumps to exhaust the excess air at a constant rate. The balance of the flows through the fast flow dilution system was evaluated and controlled at the beginning of each experiment to assure proper transfer of the sample to the instruments and also to confirm that the dilution system was operated under consistent temperature and pressure conditions. The Reynolds number for the dilution system was estimated to be 1.8×10^2 , indicating laminar flow conditions (Hinds 1999).

At the end of the dilution system there was a stainless steel cylinder acting as a mixing chamber with a total volume of 4 L (50 cm long; 10 cm diam.). The average residence time of the sample flow in the dilution tube was estimated to be 21 s, while the residence time in chamber was about 1.3 min. The sample was delivered at the bottom of the chamber via a 0.25 cm O.D. stainless steel tubing while all the instruments were connected to separate individual

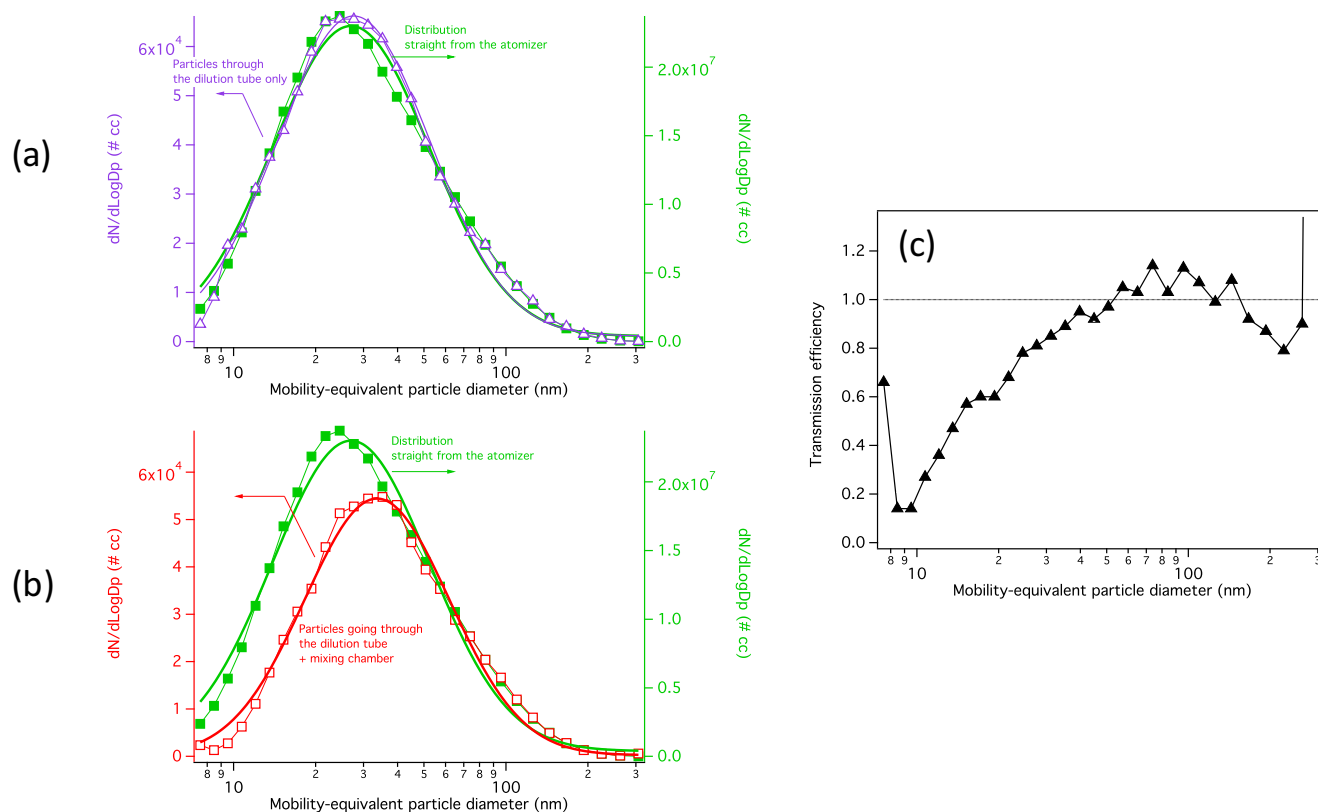
outlets at the top of the chamber. This ensured proper mixing of the sample and accomplished some “averaging” of the puffs to make more consistent aerosol size distribution measurements.

(b) Particle transmission efficiency through the dilution system. In order to determine the transmission efficiency of particles through the fast flow dilution system, particles were generated using a constant output atomizer (TSI, model 3076) containing a mixture of 2:1 dimethylamine/sulfuric acid in water (DMA, Aldrich, 40% wt. in water; H₂SO₄, Fisher Scientific, 96.2%). A pressure of ~20 psig of dry clean air was used at the inlet of the atomizer and a flow of ~2.8 L min⁻¹ exited the atomizer and passed through a NAFION™ membrane drier (Perma Pure LLC, model FC 125-240-5MP) to dry the particles. A fraction of this dry aerosol flow (~0.1 L min⁻¹) was diluted with 1.4 L min⁻¹ of dry clean air and sampled first through the fast flow dilution system in absence of the two-valve delivery system using the scanning mobility particle sizer (SMPS), described above. In this case, only the SMPS was connected to the mixing chamber located at the end of the fast flow dilution system drawing a total of ~1.5 L min⁻¹ throughout. The two-stage dilution air was reduced to 10.5 L min⁻¹ and ~6.0 L min⁻¹ for the dilution stages 1 and 2, respectively. In addition, those experiments were carried out with an ultrafine condensation particle counter (TSI Inc., model 3025A) instead of a model 3760 particle counter as described below. The following flow rates were used for the SMPS: 1.5 L min⁻¹ aerosol flow, 10 L min⁻¹ sheath flow.

The transmission efficiency (TE) of the particles through the dilution tube itself was observed to be high [TE(dil. tube) ~ 1] at all diameters (Figure S2a) while the mixing chamber showed reduced TE for the particles with diameter smaller than 50 nm (Figure S2b). The

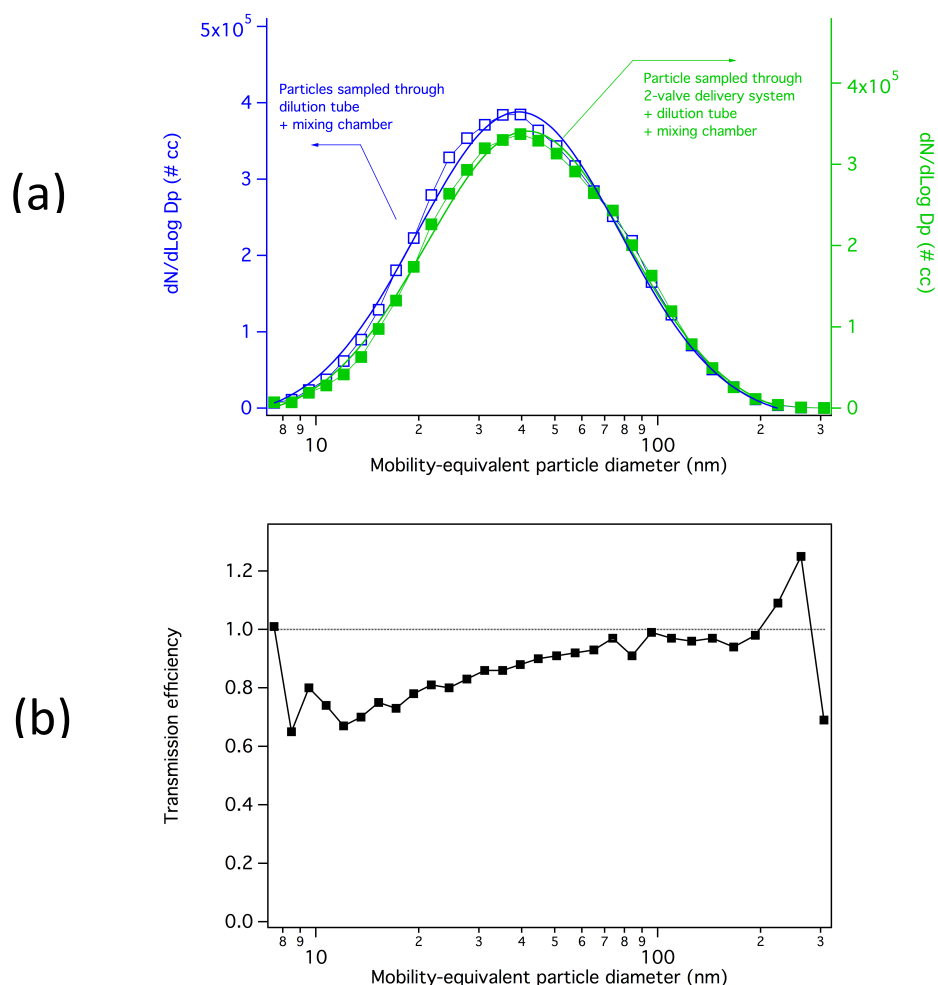
resulting transmission efficiency curve for the chamber without the two-valve delivery system was determined as the ratio of the size distribution measured with the mixing chamber to the size distribution measured without (Figure S2c).

Figure S2. Size distributions of 2:1 DMA:H₂SO₄ particles measured at the atomizer output (no dilution; green trace) and (a) after the dilution tube (no mixing chamber; purple trace), (b) after the dilution chamber (red trace). (c) Resulting transmission efficiency of mixing chamber. Particles from a mixture of 2:1 DMA/H₂SO₄ were generated using a constant output atomizer. A fraction of the outlet flow of the atomizer (0.1 L min⁻¹) was atomized with 1.4 L min⁻¹ of dry clean air before been sampled using the dilution system.



Then, the two-valve delivery system was added and its efficiency curve determined using only one channel (no puff). For these experiments, no dilution of the output of the atomizer was used prior to sampling using the dilution system. Figure S3 shows the resulting size distribution and transmission efficiency of the two-valve delivery system determined as the ratio of the size distribution measured with the two-valve delivery system to the size distribution measured without.

Figure S3. Size distributions of 2:1 DMA:H₂SO₄ particles measured after the dilution tube + mixing chamber (blue trace) and after the two-valve delivery system + dilution tube + mixing chamber (green trace). (b) Resulting transmission efficiency of the two-valve delivery system. Particles from a mixture of 2:1 DMA/H₂SO₄ solution were generated using a constant output atomizer. A fraction of the outlet flow of the atomizer (1.4 L min⁻¹) was sampled using the dilution system (no dilution prior sampling).

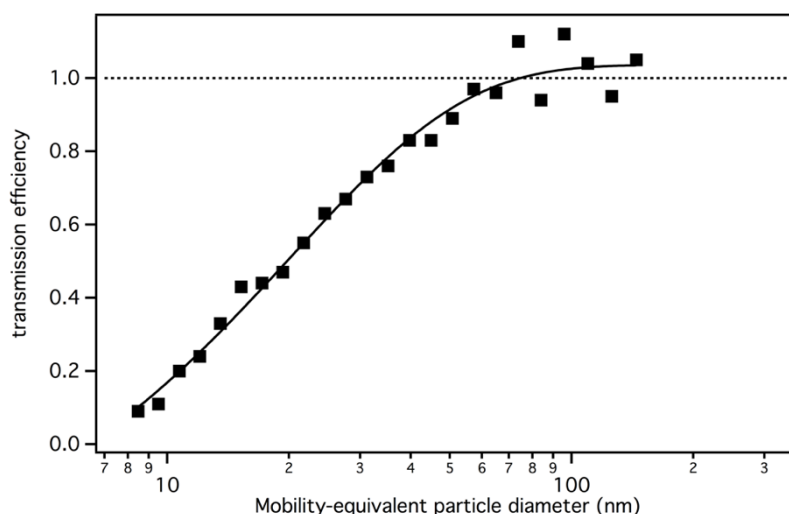


The overall transmission efficiency, $TE(overall)$, was then obtained as:

$$TE(overall) = TE(dil. tube) \times TE(chamber) \times TE(two - valve system)$$

The resulting overall transmission efficiency through the entire system is shown in Figure S4 and demonstrates excellent transmission for particles larger than 50 nm ($TE(overall) > 89\%$).

Figure S4. Overall transmission efficiency (TE) of the dilution system calculated from equation $TE(overall) = TE(dil. tube) \times TE(chamber) \times TE(two - valve system)$.



3. Waterpipe Mainstream Smoke Sampling

Relative humidity and temperature were monitored continuously using two probes (Vaisala Corp., model HMP110) located at the entrance of the two-valve system (sampling mainstream smoke from the waterpipe) and at the mixing chamber (after two-stage dilution with dry purified air). A carbon monoxide (CO) monitor (Thermo Fisher Scientific, model 48i) was used to monitor the CO levels in the mainstream emission of the waterpipe after the two-stage dilution (flow rate $\sim 0.45 \text{ L min}^{-1}$). Calibration of the instrument was performed using a

standard gas mixture containing 8.99 ppm CO in helium (Praxair Corp.), and a calibration factor of 1.08 was determined.

Size distributions of the particles emitted in the mainstream of the waterpipe were measured using a scanning mobility particle sizer (SMPS) composed of an electrostatic classifier (TSI, Inc., model 3080L), featuring a long differential mobility analyzer (DMA; TSI Inc., model 3081), combined with a condensation particle counter (CPC) (TSI, Inc., model 3760). Aerosol was sampled from the mixing chamber at a flow rate of 1.5 L min^{-1} and the sheath air of the DMA was 5 L min^{-1} with voltage scanned from 5V-10kV, allowing a distribution over the mobility diameter range of 4 to 500 nm to be measured. A one-directional scan time of 60 s was used. Instrument control and data acquisition were performed using software written in the LabView programming language (National Instruments Corp.). The inversion to the actual particle size distribution was performed using a modified version of the Washington State University SMPS Data Inversion Toolkit written in the Igor Pro programming language (Wavemetrics, Inc.). Even with the efforts to dilute the mainstream smoke, the CPC was not always able to count particles rapidly enough for the high concentrations measured. Poisson counting statistics were used to correct the data when this saturated counting condition was apparent.

The chemical composition of ultrafine particles from the diluted mainstream waterpipe smoke was measured using TDCIMS (Lawler et al. 2018; Smith et al. 2004). The instrument had an inlet flow rate of $\sim 1.5 \text{ L min}^{-1}$ and is equipped with a time-of-flight mass spectrometer with a resolving power of ~ 3500 (Tofwerk AG, model HTOF). For these experiments a bipolar aerosol neutralizer was used to charge the sampled aerosol because the unipolar chargers used typically with TDCIMS suffered from leaks caused by the pressure drop induced by the dilution

system. This limited our ability to isolate size-dependent composition, so we report composition typical of sub-100 nm particles. Polydispersed particles were collected for 2-10 min on the tip of a Pt wire by electrostatic precipitation. Typical estimated sample mass was 0.2-1.4 ng, based on characterization of size-resolved collection efficiency using atomized aerosol and the measured aerosol size distributions during the experiments. The collected particles were subsequently thermally desorbed over a 1-min temperature ramp and soak from room temperature to $\sim 600^{\circ}\text{C}$. Positive ion mode was recorded for all experiments, corresponding to chemical ionization of desorbed nanoparticle constituents using $(\text{H}_2\text{O})_n\text{H}_3\text{O}^+$ ($n=1-3$) reagent ions, forming H^+ adducts of closed-shell molecules, i.e. $[\text{M}+\text{H}]^+$.

Real-time measurements of the organic gases from the diluted mainstream smoke were performed using a high resolution PTR-ToF-MS (Ionicon Analytik, PTR-ToF-MS 8000). The operating principle of the PTR-ToF-MS has been described previously (Jordan et al. 2009). Briefly, volatile organic compounds sampled by the instrument can undergo proton transfer reaction with the H_3O^+ reagent, forming primarily $[\text{M} + \text{H}]^+$ ions if the proton affinity of the analyte is higher than that of water. The instrument was operated with a drift voltage, temperature and pressure of 600 V, 60°C and 2.2 mbar respectively (resulting in a ratio of the electric field (E) to the number density of the drift tube buffer gas molecules (N) of $E/N \sim 135$ Td where $1 \text{ Td} = 10^{-17} \text{ V cm}^2$) and a flow rate of 0.1 L min^{-1} through 1.59 mm O.D. PEEK tubing inlet heated at 70°C . The data were acquired using a 1 s time resolution. Mass-to-charge calibration was verified at the beginning of each experiment using four isotopic ions including $\text{H}_3^{18}\text{O}^+$ at m/z 21.022, $^{16}\text{O}^{18}\text{O}^+$ at m/z 33.994, $(\text{H}_2\text{O})\text{H}_3^{18}\text{O}^+$ at m/z 39.033 and acetone at m/z 59.049 ($[\text{M} + \text{H}]^+$) from room air. In addition, headspace over pure 1,3-diiodobenzene (98%, Sigma-Aldrich)

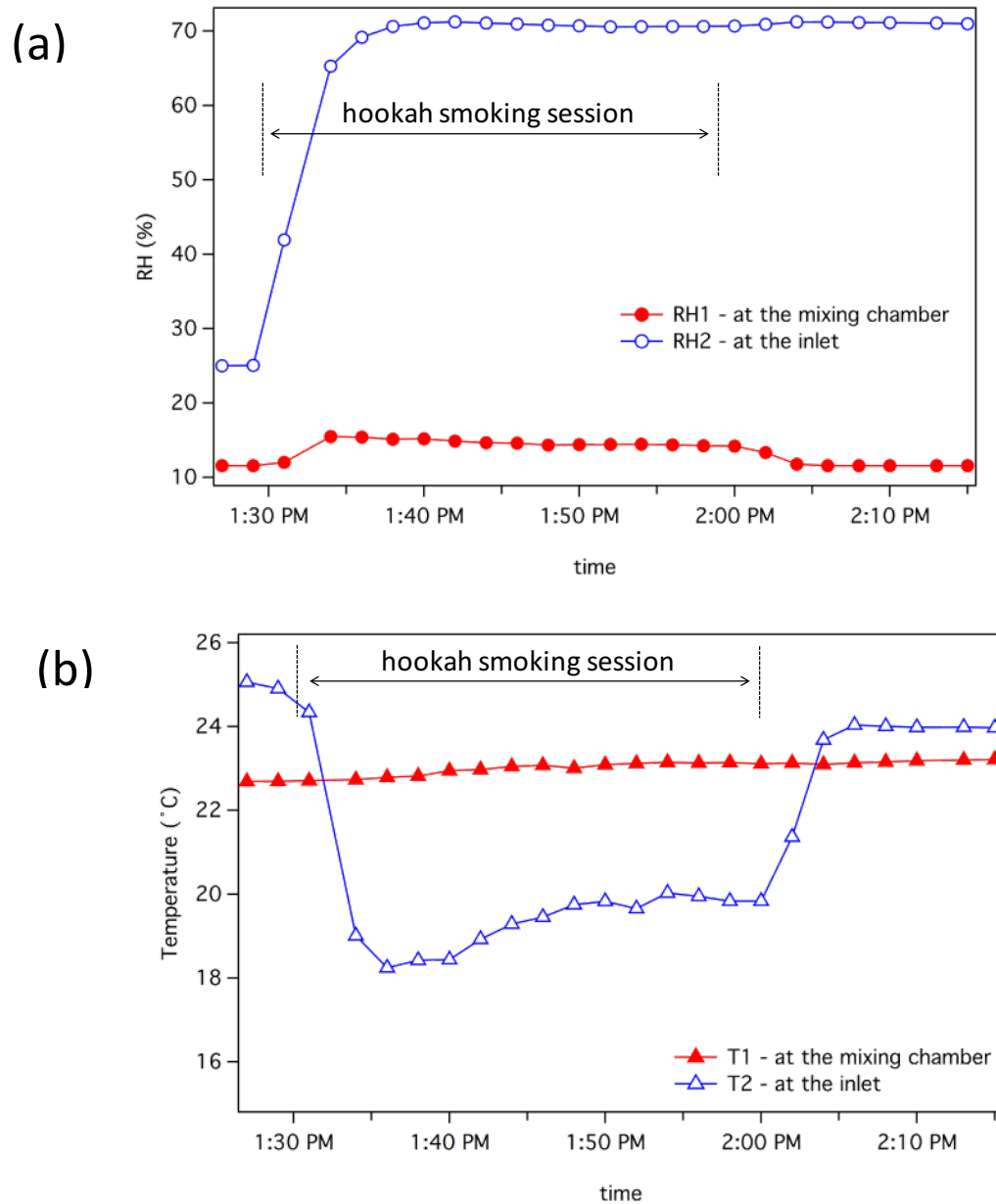
was sampled at the beginning of some experiments to mass calibrate the higher range of mass-to-charge values using its corresponding fragment ion at m/z 203.943 ($[C_6H_4I_2 + H - I]^+$) (Stockwell et al. 2015).

4. Reference Cigarette Smoking Protocol

The cigarettes were conditioned at a relative humidity of ~60% by maintaining them enclosed in a desiccator above a ~75% wt. aqueous glycerol solution for at least 48 h prior to use. The inlet of the dilution system was slightly modified to make it possible to smoke the cigarette artificially using a puff flow of $\sim 1 \text{ L min}^{-1}$ that was combined with dry purified air to make a total of $\sim 3 \text{ L min}^{-1}$ as required by our instrument suite. The cigarette was lit using an electronic lighter for the duration of the first puff and a total of 7 puffs were smoked for each cigarette (2 s puff; every 60 s). The total dilution factor of the cigarette emission sampled through the entire system including the 2-stage active dilution and the puff time step (2 s puff; 58 s purified air) was ~ 3250 .

5. Relative Humidity and Temperature Profiles During Waterpipe Smoking

Figure S5. Representative relative humidity (RH) time profile (a) and temperature profile (b) obtained during a waterpipe smoking session with the conventional tobacco. Each data point corresponds to the average value of RH and temperature measured over two-minute time intervals. The blue opened data points correspond to measurements at the exit of the waterpipe hose (before the dilution tube) and the red filled data points correspond to measurements at the mixing chamber.



6. Online Measurements of Volatile Organic Compounds by PTR-ToF-MS

Figure S6. Typical unit mass resolution PTR-ToF-MS mass spectra from the waterpipe mainstream smoke of the three tobaccos investigated including (a) the conventional tobacco, (b) the nicotine-free herbal tobacco and (c) the dark leaf unwashed tobacco, and (d) the 3R4F reference cigarette. All spectra were collected at the end of the smoking session (the last 10 puffs for the waterpipe samples, and the last puff for the cigarette sample) and the background signal has been subtracted out. The peaks indicated with a star correspond to the O_2^+ ion at m/z 32 and the hydronium ion - water complex $(H_2O)_2H^+$ at m/z 37 that did not subtract out completely.

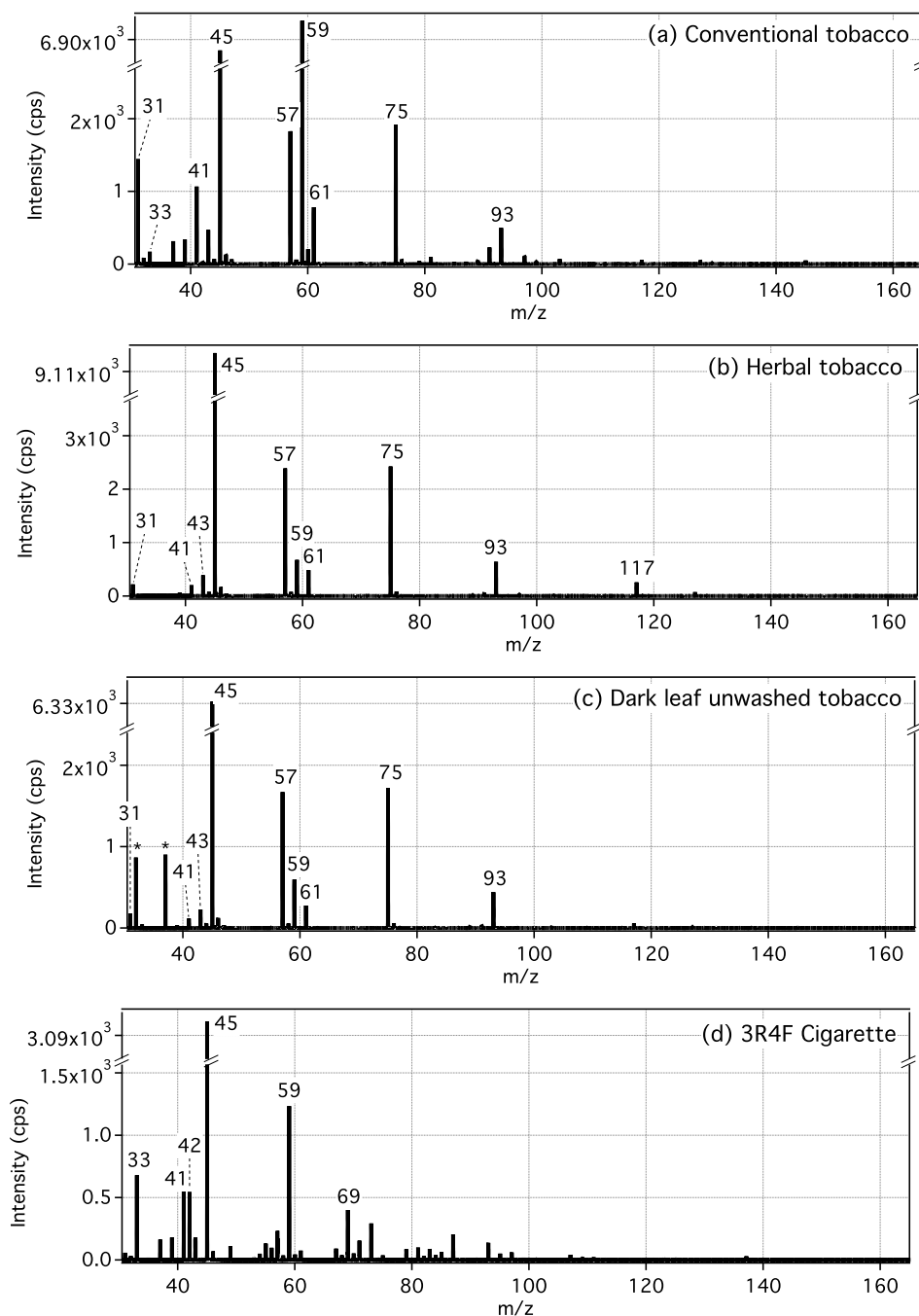


Figure S7. Expanded view of the PTR-ToF-MS spectra showing the separation of multiple peaks observed at nominal m/z 42, 43, 47, 57, 69, 91, 93, 107, 129 and 163. The red trace corresponds to the sample, while the blue trace is the background.

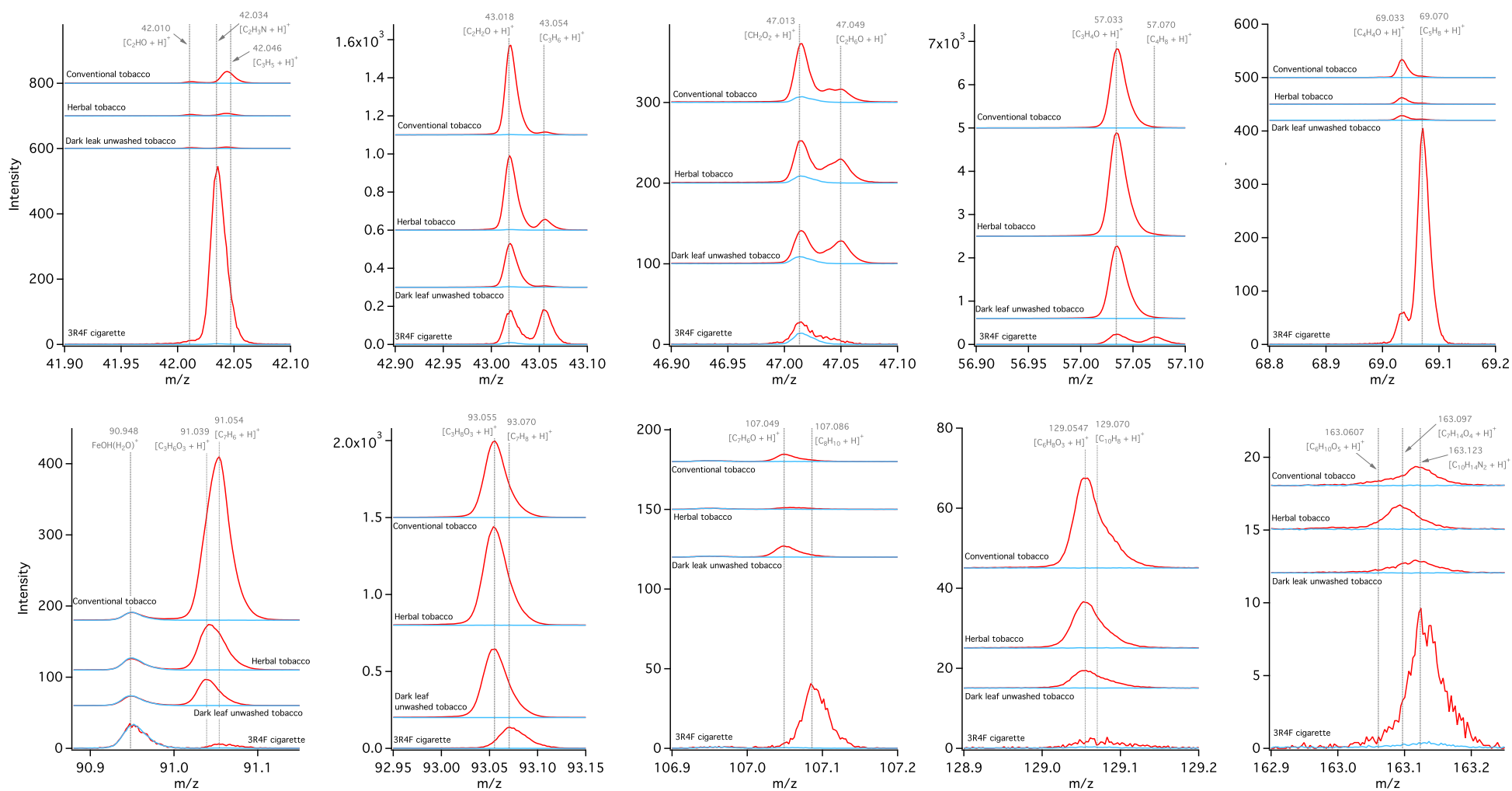


Table S1. Relative ion distribution normalized to m/z 45 (acetaldehyde) for waterpipe experiment with glycerol only and all three investigated tobaccos. Numbers in parentheses for the conventional tobacco, the nicotine-free herbal tobacco mixture and the dark leaf unwashed tobacco represent one standard deviation of n replicate measurements.

Nominal m/z	Assignment	Glycerol only (n = 1)	Conventional (n = 4)	Herbal (n = 2)	Dark leaf (n = 2)
31	$[\text{CH}_2\text{O}+\text{H}]^+$	0.53	0.23 (0.007)	0.02 (0.002)	0.03 (0.004)
33	$\text{CH}_4\text{O}+\text{H}^+$	0.12	0.02 (0.002)	0.01 (0.000)	0.01 (0.000)
41	$[\text{C}_3\text{H}_4+\text{H}]^+$	0.09	0.17 (0.006)	0.02 (0.001)	0.02 (0.003)
43	$[\text{C}_2\text{H}_2\text{O}+\text{H}]^+$	0.37	0.07 (0.006)	0.04 (0.001)	0.04 (0.002)
45	$[\text{C}_2\text{H}_4\text{O}+\text{H}]^+$	1	1	1	1
57	$[\text{C}_3\text{H}_4\text{O}+\text{H}]^+$	0.23	0.26 (0.008)	0.25 (0.002)	0.27 (0.002)
59	$[\text{C}_3\text{H}_6\text{O}+\text{H}]^+$	0.16	1.09 (0.110)	0.08 (0.007)	0.10 (0.014)
61	$[\text{C}_2\text{H}_4\text{O}_2+\text{H}]^+$	0.66	0.10 (0.011)	0.05 (0.000)	0.05 (0.004)
75	$[\text{C}_3\text{H}_6\text{O}_2+\text{H}]^+$	0.20	0.28 (0.008)	0.26 (0.001)	0.27 (0.001)
93	$[\text{C}_3\text{H}_8\text{O}_3+\text{H}]^+$	0.004	0.07 (0.003)	0.07 (0.000)	0.07 (0.000)

Figure S8. Typical unit mass resolution mass spectra obtained using the PTR-ToF-MS from the waterpipe mainstream smoke of (a) only charcoal + water conditions (no tobacco), (b) the conventional tobacco without charcoal (no heat) and (c) glycerol only (no tobacco). All spectra were collected at the end of the smoking session (the last 10 puffs for the waterpipe samples) and the background signal has been subtracted out. Spectra (d) resulted from nebulized glycerol aqueous particles generated using a hospital nebulizer (MicroMist nebulizer; Hudson RCI®). The peaks indicated with a star corresponds to the O_2^+ ion at m/z 32 and the hydronium ion - water complex $(H_2O)_2H^+$ at m/z 37 that did not subtract out completely.

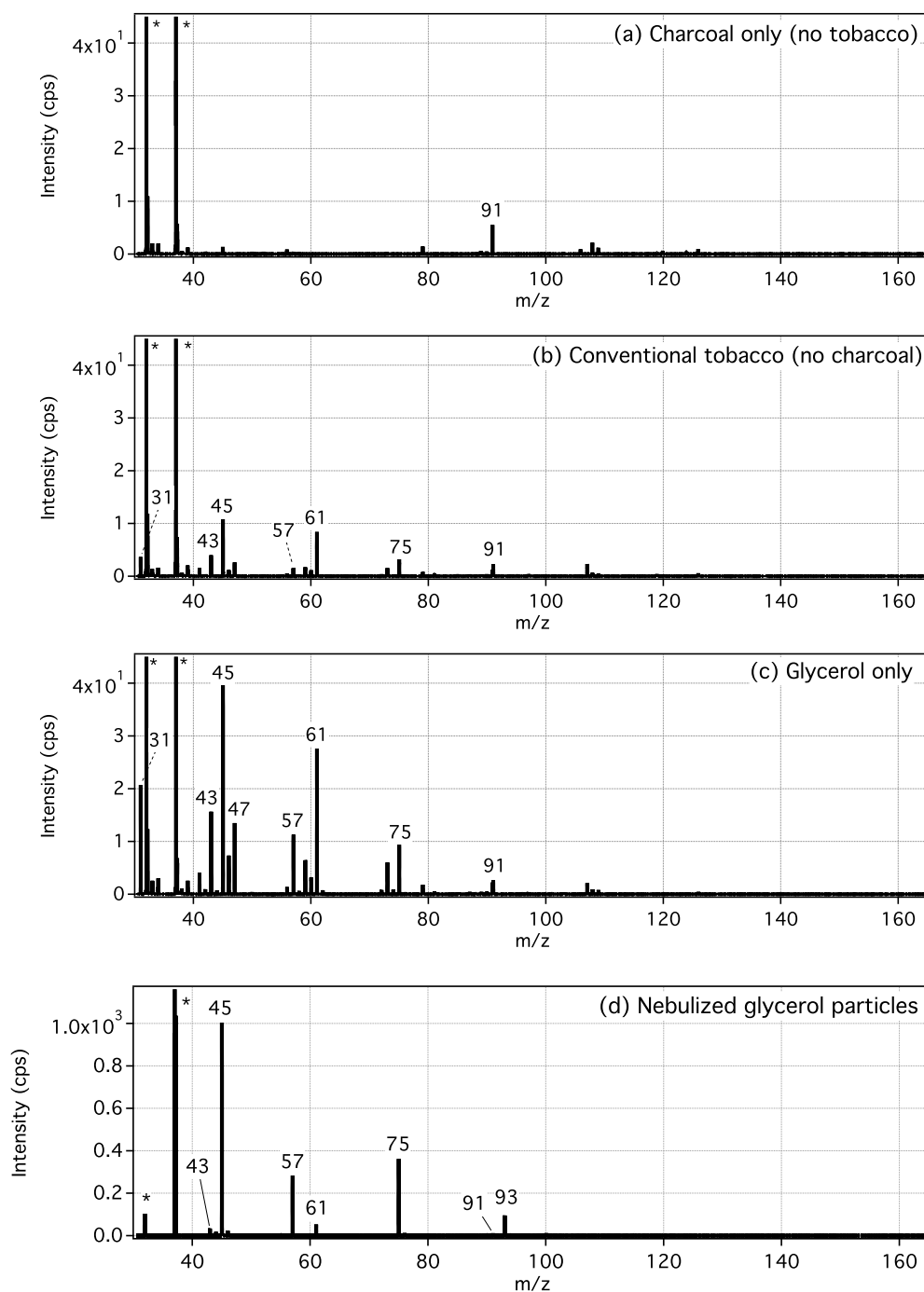


Figure S9. Expanded view of the PTR-ToF-MS spectra showing m/z 79 for the conventional tobacco mixture (red trace), the herbal tobacco (orange trace), the dark leaf unwashed tobacco (green trace) compared to the charcoal only (no tobacco) experiment. For comparison, the conventional tobacco without charcoal (pink trace), the glycerol only (dark blue trace) experiments and the 3R4F reference cigarette (light blue trace) are also shown. All spectra are background subtracted.

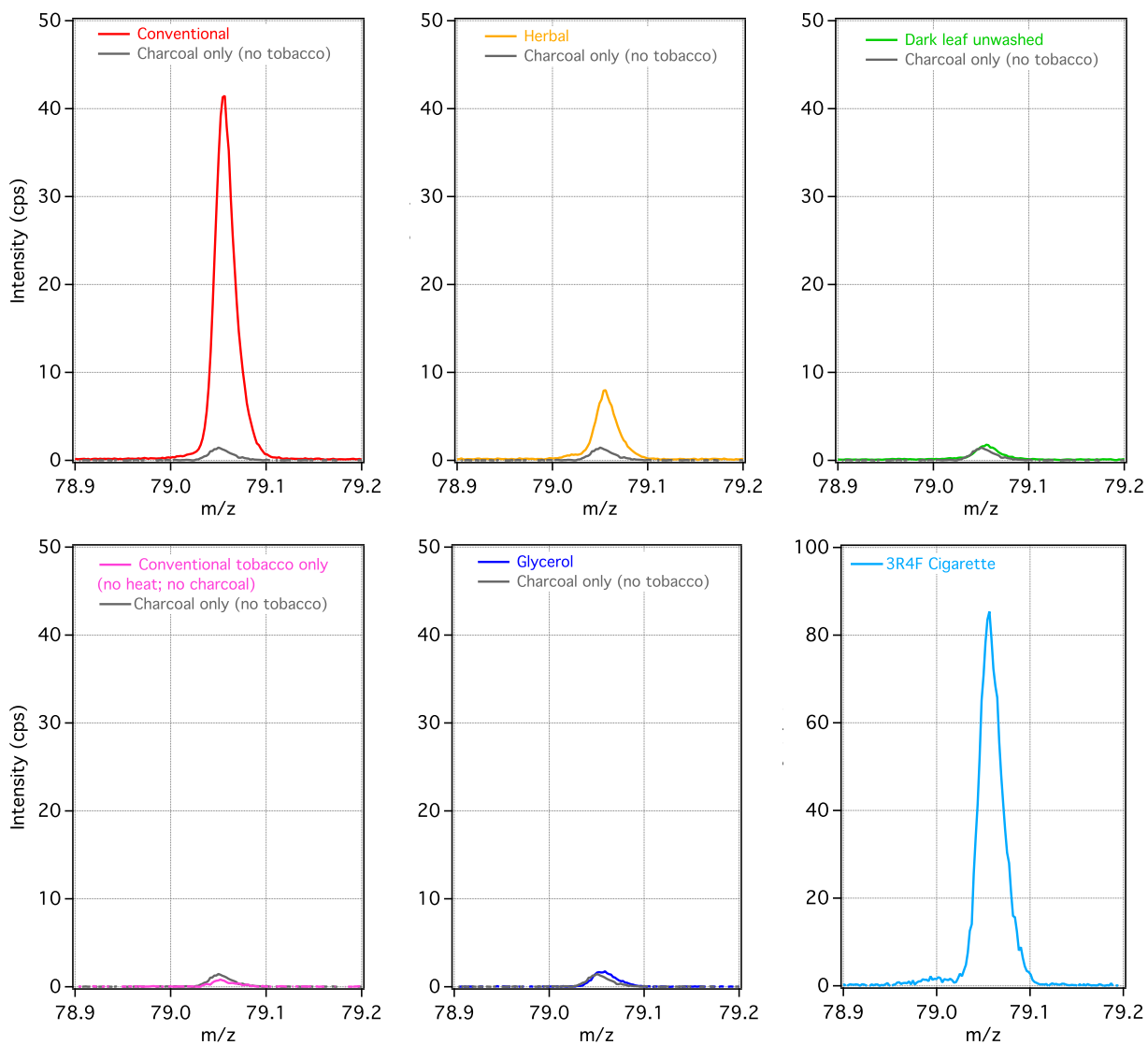


Figure S10. Comparison of averaged unit mass resolution PTR-ToF-MS mass spectra as a function of smoking time. Each spectrum corresponds to an average of spectra taken over 10 puffs (5 min). Conventional tobacco run performed (a) under 'normal' condition (charcoal + water + shisha) and (b) without water in the waterpipe bowl. All spectra are background subtracted. Negative peaks correspond to m/z 32 (O_2^+) and 37 ($(H_2O)_2H^+$) incompletely removed by the subtraction.

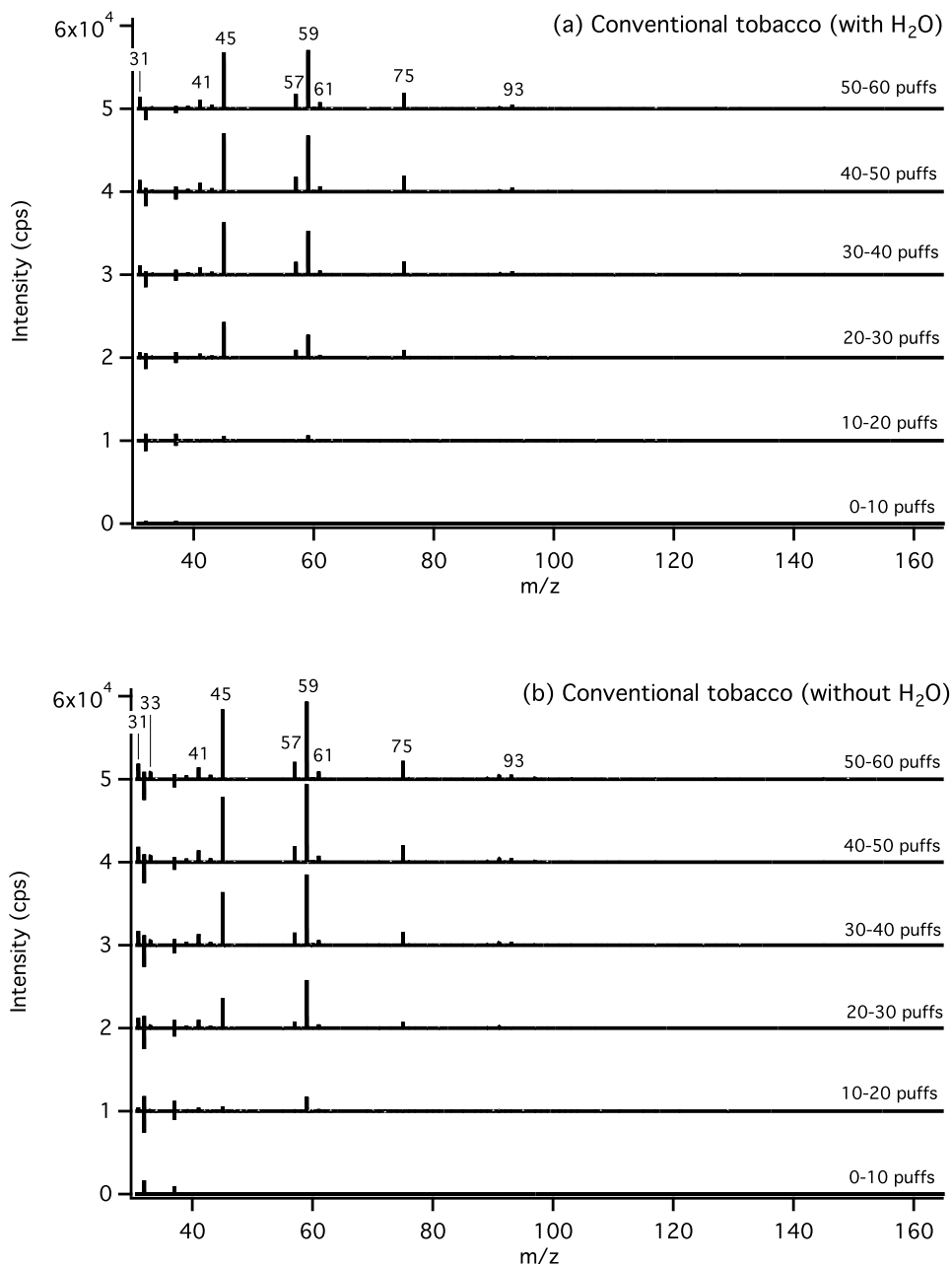
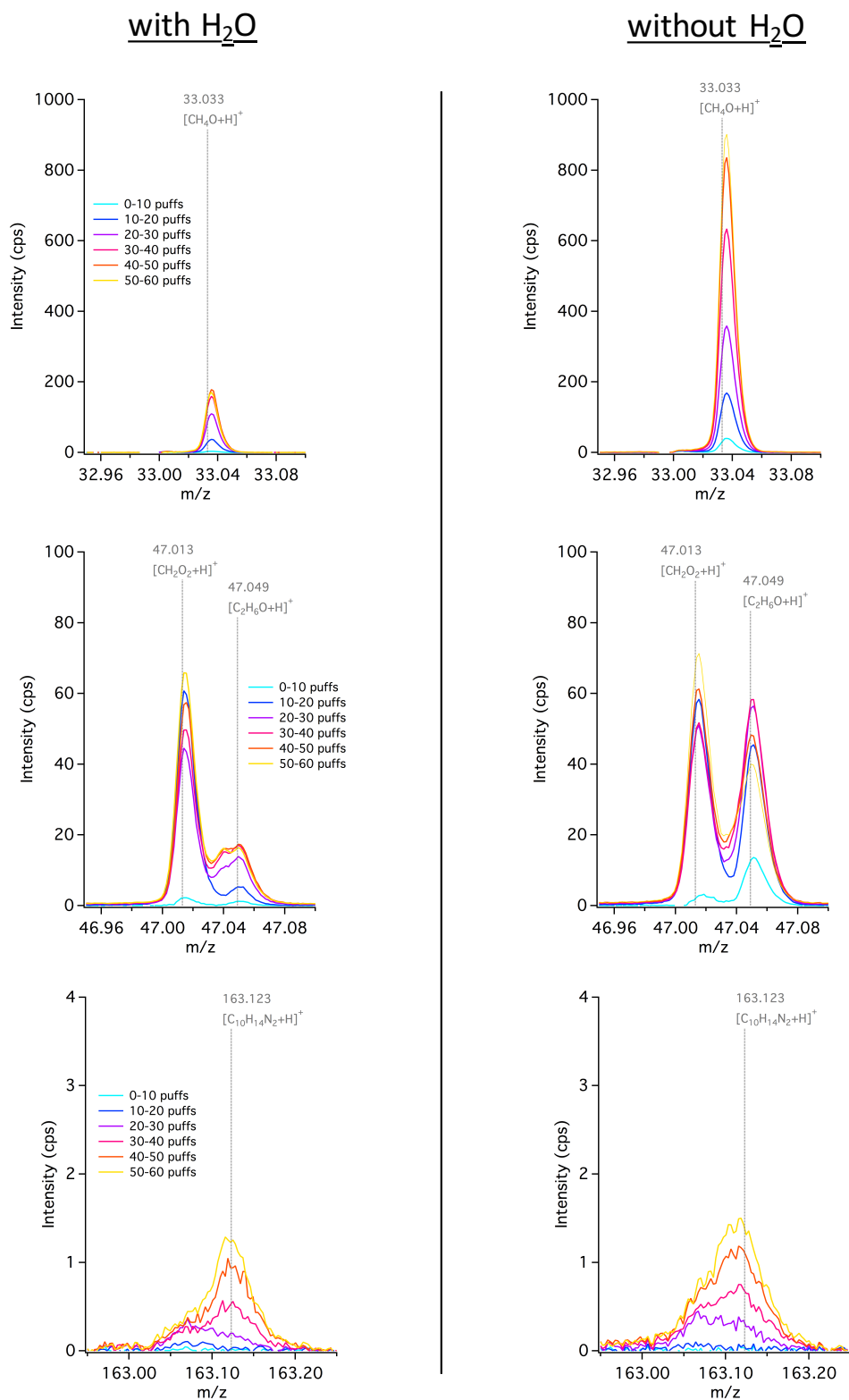
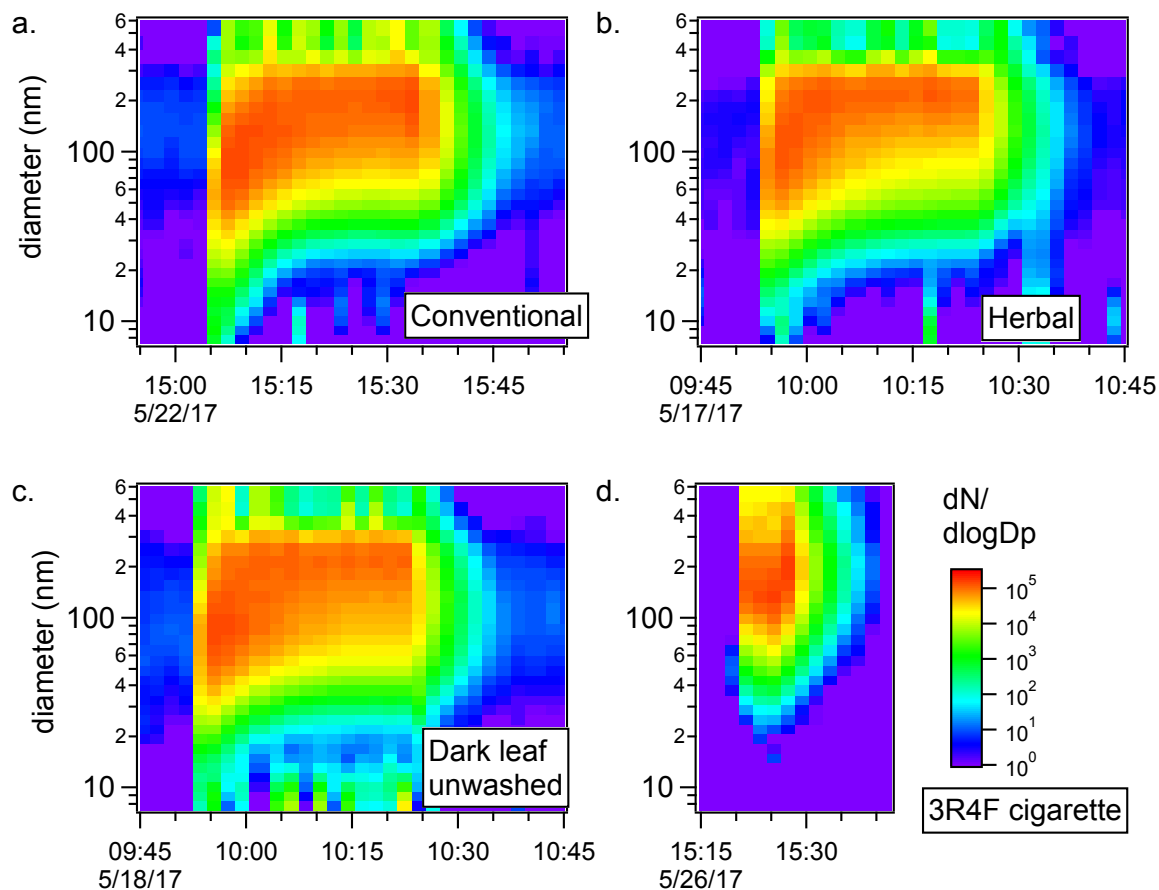


Figure S11. Expanded view of the PTR-ToF-MS spectra collected for the conventional tobacco (with and without water present in the waterpipe bowl) showing the evolution of the signal at nominal m/z 33, 47 and 163 as a function of time (number of puffs). Each spectrum corresponds to an average over 10 puffs and is background subtracted.



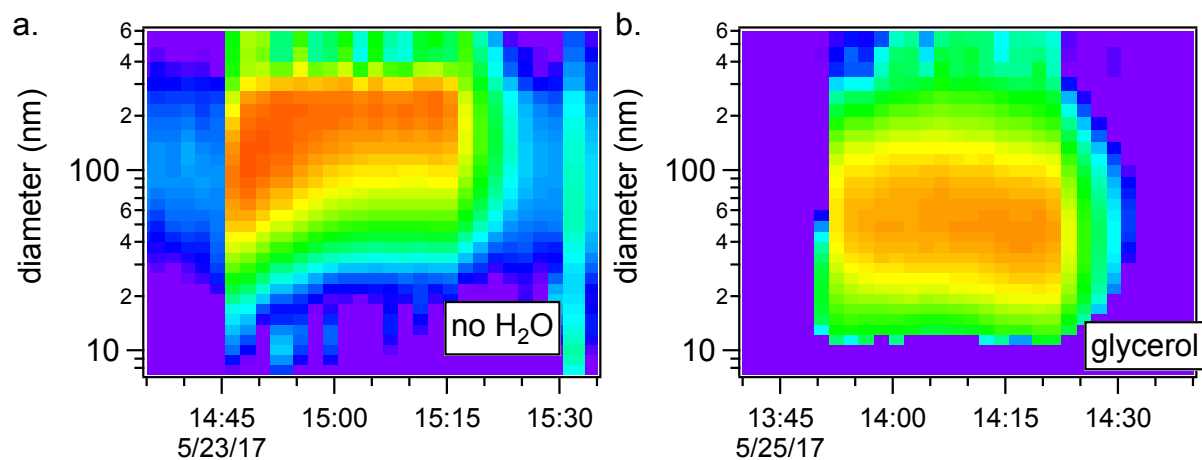
7. Size Distribution Measurements

Figure S12. Typical size distributions for individual smoking sessions measured for three different shishas including (a) the conventional tobacco, (b) the nicotine-free herbal tobacco, and (c) the dark leaf unwashed tobacco, as well as a 3R4F reference cigarette (d). Concentrations are corrected for dilution and size-dependent sampling losses through the experimental system. The start of the smoking session corresponds to the sudden increase on the particle number concentration.



In absence of charcoal (no heat), no particles were observed. Because of their similarities, particle size distribution results from 'charcoal only' and 'glycerol only' experiments are averaged together and the resulting averaged distribution is presented in Figure S13b. This similarity suggests that the major tobacco additive glycerol is not the primary driver of new particle formation or growth in hookah smoke aerosol.

Figure S13. Size distribution of particles measured from hookah mainstream smoke collected (a) in absence of water in the waterpipe bowl (conventional tobacco), and (b) during an experiment where the tobacco was replaced with 10 g of glycerol. Intensity scale is the same as in Figure 3 in the main manuscript.



8. TDCIMS Measurements

Figure S14. Size-binned sample mass collected (ng) from the hookah mainstream smoke by the TDCIMS for a typical hookah experiment.

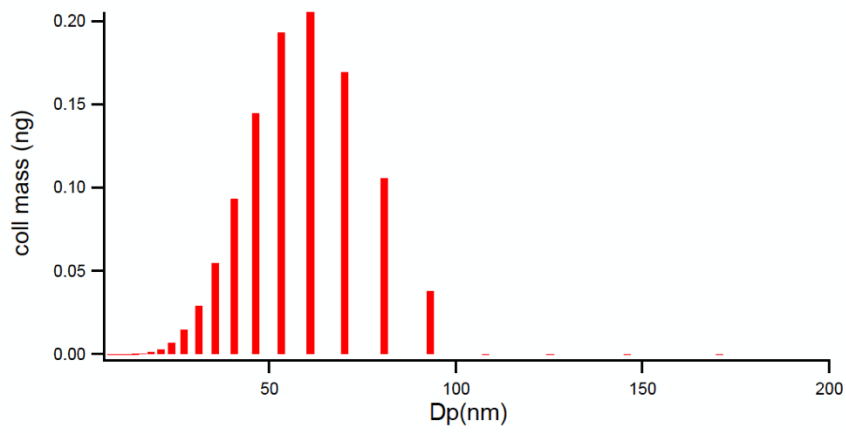


Figure S15. TDCIMS mass spectra of ultrafine particles collected from hookah mainstream smoke from (a) the conventional tobacco, (b) the nicotine-free herbal tobacco, (c) the dark leaf unwashed tobacco, and (d) the 3R4F reference cigarette. Formulas next to the peaks are given in their detected ionic form (as an H^+ adduct), with the charge symbol dropped to avoid clutter. The presented mass spectra are averages of two to four experiments performed using the same tobacco, with error bars corresponding to one standard error of the mean. Labeled ions are “detectable” by the criteria that their background-subtracted abundances are either two standard errors greater than zero for the average, or if they were two standard errors above zero for every individual experiment. Only detectable ions above 0.7% of the total signal are labeled. Glycerol and its clusters were excluded because of variable and large gas phase backgrounds. The range of the m/z axis is chosen to highlight likely molecular (unfragmented) species with high confidence of formula identification.

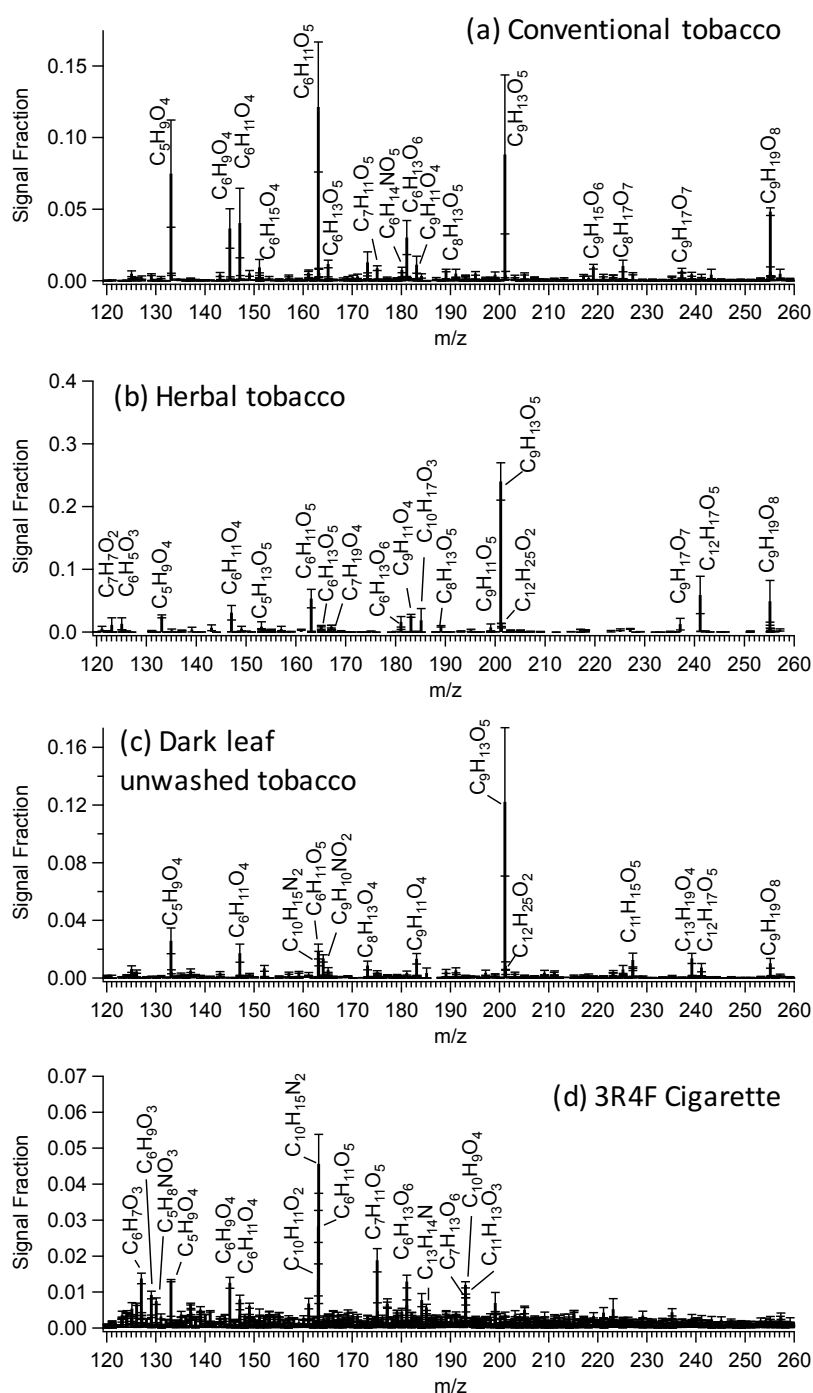
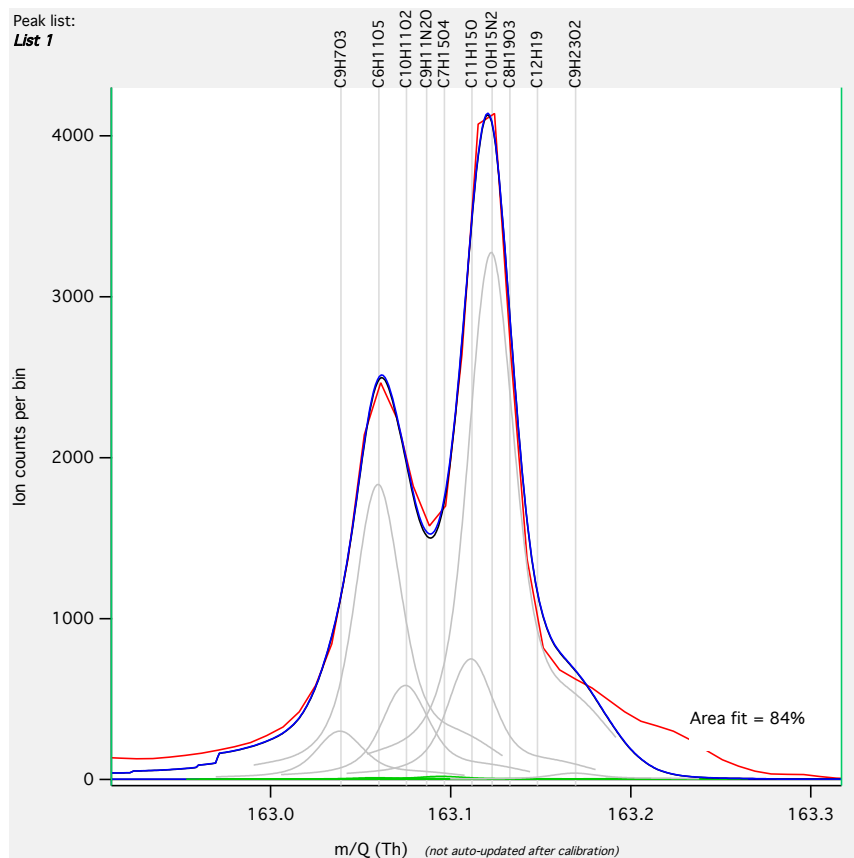


Figure S16. High resolution peak fitting of nominal m/z 163 for the raw averaged mass spectrum of non-background-corrected signal from a cigarette smoking experiment. $C_6H_{11}O_5^+$ (levoglucosan) and $C_{10}H_{15}N_2^+$ (nicotine) are the main contributors to the spectrum.



References

- Blair, S. L., S. A. Epstein, S. A. Nizkorodov, N. Staimer. 2015. A real-time fast-flow tube study of VOC and particulate emissions from electronic, potentially reduced-harm, conventional, and reference cigarettes. *Aerosol Sci. Tech.* 49:816-827. doi: 10.1080/02786826.2015.1076156.
- Hinds, W. C. 1999. *Aerosol Technology: Properties, Behavior, and Measurement of Airborne Particles, 2nd Edition*. New York: John Wiley & Sons.
- Jordan, A., S. Haidacher, G. Hanel, E. Hartungen, L. Mark, H. Seehauser, R. Schottkowsky, P. Sulzer, T. D. Mark. 2009. A high resolution and high sensitivity proton-transfer-reaction time-of-flight mass spectrometer (PTR-TOF-MS). *Int. J. Mass spectrom.* 286:122-128. doi: 10.1016/j.ijms.2009.07.005.
- Lawler, M. J., M. P. Rissanen, M. Ehn, R. L. Mauldin, N. Sarnela, M. Sipila, J. N. Smith. 2018. Evidence for diverse biogeochemical drivers of boreal forest new particle formation. *Geophys. Res. Lett.* 45:2038-2046. doi: 10.1002/2017gl076394.
- Shihadeh, A., T. Eissenberg, M. Rammah, R. Salman, E. Jaroudi, M. El-Sabban. 2014. Comparison of tobacco-containing and tobacco-free waterpipe products: Effects on human alveolar cells. *Nicotine Tob. Res.* 16:496-499. doi: 10.1093/ntr/ntt193.
- Shihadeh, A., R. Salman, E. Jaroudi, N. Saliba, E. Sepetdjian, M. D. Blank, C. O. Cobb, T. Eissenberg. 2012. Does switching to a tobacco-free waterpipe product reduce toxicant intake? A crossover study comparing CO, NO, PAH, volatile aldehydes, "tar" and nicotine yields. *Food Chem. Toxicol.* 50:1494-1498. doi: 10.1016/j.fct.2012.02.041.
- Smith, J. N., K. F. Moore, P. H. McMurry, F. L. Eisele. 2004. Atmospheric measurements of sub-20 nm diameter particle chemical composition by thermal desorption chemical ionization mass spectrometry. *Aerosol Sci. Tech.* 38:100-110. doi: 10.1080/02786820490249036.
- Stockwell, C. E., P. R. Veres, J. Williams, R. J. Yokelson. 2015. Characterization of biomass burning emissions from cooking fires, peat, crop residue, and other fuels with high-resolution proton-transfer-reaction time-of-flight mass spectrometry. *Atmos. Chem. Phys.* 15:845-865. doi: 10.5194/acp-15-845-2015.